Advanced Optical Diagnostics for Ice Crystal Cloud Measurements in the NASA Glenn Propulsion Systems Laboratory

Timothy J. Bencic[*], Amy F. Fagan[†], Judith F. Van Zante[‡]
NASA Glenn Research Center, Cleveland, Ohio, 44135

Jonathan P. Kirkegaard[§]
Jacobs Technology, Cleveland, Ohio 44135

David P. Rohler[**], Arjun Maniyedath[††]
Plexar Associates, Inc., Shaker Heights, OH 44122

and

Steven H. Izen[‡‡]
Case Western Reserve University, Cleveland, OH 44106

A light extinction tomography technique has been developed to monitor ice water clouds upstream of a direct connected engine in the Propulsion Systems Laboratory (PSL) at NASA Glenn Research Center (GRC). The system consists of 60 laser diodes with sheet generating optics and 120 detectors mounted around a 36-inch diameter ring. The sources are pulsed sequentially while the detectors acquire line-of-sight extinction data for each laser pulse. Using computed tomography algorithms, the extinction data are analyzed to produce a plot of the relative water content in the measurement plane. To target the low-spatial-frequency nature of ice water clouds, unique tomography algorithms were developed using filtered backprojection methods and direct inversion methods that use Gaussian basis functions. With the availability of *a priori* knowledge of the mean droplet size and the total water content at some point in the measurement plane, the tomography system can provide near real-time *in-situ* quantitative full-field total water content data at a measurement plane approximately 5 feet upstream of the engine inlet. Results from ice crystal clouds in the PSL are presented. In addition to the optical tomography technique, laser sheet imaging has also been applied in the PSL to provide planar ice cloud uniformity and relative water content data during facility calibration before the tomography system was available and also as validation data for the tomography system. A comparison between the laser sheet system and light extinction tomography resulting data are also presented. Very good agreement of imaged intensity and water content is demonstrated for both techniques. Also, comparative studies between the two techniques show excellent agreement in calculation of bulk total water content averaged over the center of the pipe.

---

[*] Senior Research Engineer, Optical Instrumentation and NDE Branch, 21000 Brookpark Rd
[†] Senior Research Engineer, Optical Instrumentation and NDE Branch, 21000 Brookpark Rd, AIAA Senior Member
[‡] Icing Engineering Technical Lead, Aviation Environments Test Engineering Branch, 21000 Brookpark Rd, AIAA Senior Member
[§] Mechanical Test Engineer, Testing Branch, 21000 Brookpark Rd
[**] President, 3120 Belvoir Rd
[††] Research Scientist, 3120 Belvoir Rd
[‡‡] Professor of Mathematics, Consultant to Plexar Associates, Inc., 10900 Euclid Ave

Nomenclature

PSL	=	Propulsion System Laboratory
S	=	spray reference number
TWC	=	total water content (g/m^3)
MVD	=	median volumetric diameter (μm)
gpm	=	Spray system flow rate in gallons per minute
ND	=	Particle number density ($number/cm^3$)
CT	=	computed tomography
I	=	intensity measured by the detector
I_0	=	source intensity
l_i	=	line of sight from a source to a detector
s	=	length along the line l_i connecting a source and detector
x	=	distance along the line l_i connecting a source and detector
μ	=	attenuation coefficient

I. Introduction

THERE have been over 200 documented cases of jet engine power loss events during flight at high altitudes due to ingestion of ice particles[1]. The events typically occur at altitudes above 22,000 feet and near deep convective systems, often in tropical regions. It is recognized in the industry that supercooled liquid water does not exist in large quantities at these high altitudes and therefore it is expected that the events are due to the ingestion of ice particles. Based on this recent interest in ice particle threat to engines in flight, the NASA Glenn Research Center (GRC) installed the capability to produce ice crystal and mixed phase water clouds in the Propulsion Systems Laboratory (PSL) Test Cell 3. The ice crystal cloud operational parameters, developed with input from industry, were Median Volumetric Diameter (MVD) from 40 to 60 μm and Total Water Content (TWC) from 0.5 to 9.0 g/m^3. PSL is currently the only engine test facility that can simulate both altitude effects and an ice crystal cloud. It is a continuous flow facility that creates the temperature and pressure inlet conditions that propulsion systems experience in high-speed, high-altitude flight. Specifically for the icing system, the total temperature can be controlled between +45 to -60 F, pressure altitude from 4,000 to 40,000 feet (facility limit is 90,000 feet), and Mach from 0.15 to 0.8 (facility limit is Mach 3.0).

Advanced optical diagnostics have been developed in parallel with this effort to provide *in-situ* measurement capabilities for ice water content and cloud uniformity. The traditional, ice-accretion based methods for making these measurements in supercooled liquid water clouds are not adequate for ice crystals at high speeds. New methodologies and techniques had to be developed, and non-intrusive methods are ideal.

Various optical techniques have been applied in NASA GRC's Icing Research Tunnel (IRT) over the years[2-5]. Building on the knowledge gained from developing and applying various optical techniques in the IRT facility a light extinction tomography system has been targeted as the desired cloud diagnostic for PSL. A tomography system installed in the entrance pipe leading to the direct connected jet engine enables *in-situ* non-intrusive measurements of the impinging ice cloud during an actual engine test. The entrance ports for the sources and detectors are completely sealed and flush with the inside of the duct so as not to disturb the flow field. The system is remotely controlled and the data can be processed within seconds providing near real-time feedback to research and test engineers.

While the tomography system was being developed, a parallel effort to install a laser sheet imaging diagnostic for use during the PSL icing calibration test was completed. The laser sheet imaging system was used to acquire planar quasi-quantitative visualizations of ice and liquid water cloud content at the PSL piping exit where a jet engine would be mounted for an engine test, see Figure 1. This diagnostic system was successfully used during the calibration test and showed good agreement with water content measurements by multi-wire and robust TWC probes. Some data were acquired at the very end of the calibration test using a prototype of the light extinction tomography system installed at the PSL piping exit in the same location where the laser sheet data was acquired. The final tomography system will be installed about 5 feet upstream of this point, as shown in Figure 1, in-line with the facility piping for future engine tests. The data from the tomography system was compared with and validated against the laser sheet cloud data.

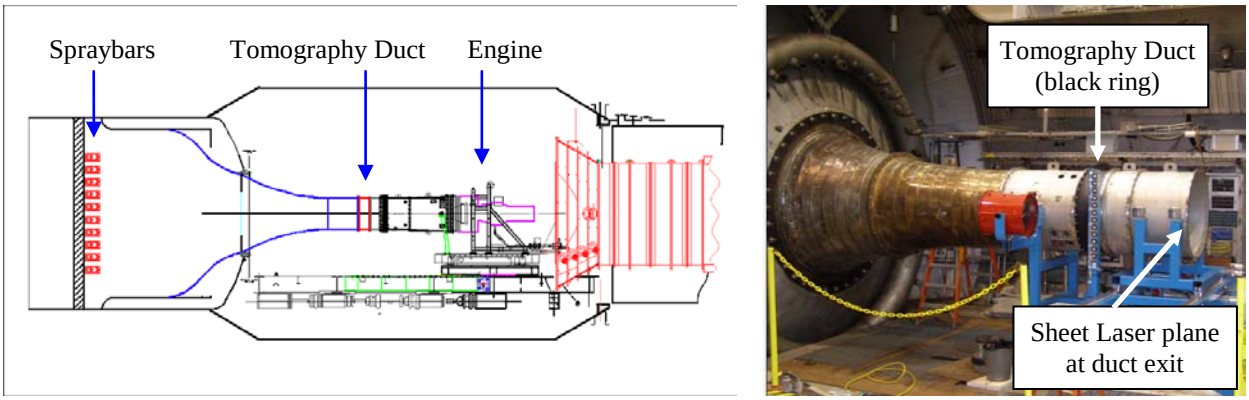

Figure 1. Schematic of PSL Cell 3 with engine and picture depicting the future location of the Tomography Duct. The sheet laser was located immediately downstream of the duct exit plane.

II. Laser Sheet Cloud Imaging

A laser sheet imaging system was installed in the PSL facility with the objective of acquiring planar qualitative and potentially quantitative visualizations of cloud water content. The ice crystal cloud was generated by the new facility spray bars in the plenum. The cloud then enters a 27:1 contraction ratio into a constant area 36" duct.

The laser sheet imaging system was an interim solution to provide water content and cloud uniformity data prior to the installation of the light extinction tomography system, and also as a means of providing validation data for comparison with the tomography results. A schematic of the system is shown in Figure 2. A 532nm 1.5W continuous wave laser that is located outside the test cell is coupled into a 50µm core step index fiber that is terminated with the sheet projection optics. The diverging sheet is collimated using a cylindrical lens that illuminates the flow field with a 24" high horizontal collimated laser sheet that is projected across the PSL duct exit. Light scattered from ice crystals and liquid water droplets is imaged with a CCD camera that is mounted normal to the sheet but under the exhaust collection piping producing a skewed image. The position of the camera is critical for a constant response from Mie scattering from the particles over the range of angles of the camera view. The skewed viewing makes it necessary for the images to be de-warped to give an undistorted map of the cloud across the duct. The de-warping image manipulation process utilizes a reference grid that is placed in the same location as the light sheet at the exit of the exit duct and skewed images of the grid are acquired. Using the skewed grid image, control points are transferred to the laser sheet images that correspond to the same locations in the reference grid image. A quadratic warping function is used to perspective correct the laser sheet images to a normal view as illustrated in Figure 3. A series of 47 images with 500ms integration time per image were acquired and averaged together to provide the results shown. The scattered light intensity gives an indication of the particle number density for a given mean particle size and hence the TWC. Contour color plots are used to display the cloud density maps across the duct exit.

Two-dimensional contour plots of the scattered light intensity are shown in Figure 4 for a series of sprays ranging from light to heavy sprays. Horizontal line profiles through the center of each of these sprays are shown in Figure 5. It is clearly evident that there is a correlation between water content and scattered light intensity. Skewing of the data due to light sheet attenuation through the spray was found to be minimal in most cases; however these data show that as the sprays get heavier, the attenuation through the cloud becomes a larger source of error, as evidenced by the biasing of the peak of the spray toward the right. In addition to characterizing the cloud by TWC[7], one can monitor precisely the water supply system flow rate introduced at the spray bars in terms of gallons per minute (gpm). Care is taken that water not hit the contraction walls. For some of the intentionally non-uniform sprays reported in this paper, the water flow rate will also be reported.

During the initial cloud characterization effort, the laser sheet data were critical in determining the bulk TWC in the duct. The TWC was directly measured with multi-wire or robust TWC probes only at the center point. The measured TWC was mated to the laser sheet intensity values at that point; that ratio was applied over the center 24" circle to convert the intensities to TWC. Figure 6 shows one example of how the laser sheet demonstrates calibrated

laser sheet spray results showing quantitative TWC obtained by calibration of the image intensity with quantitative measurements from multi-wire or robust probe measurements.

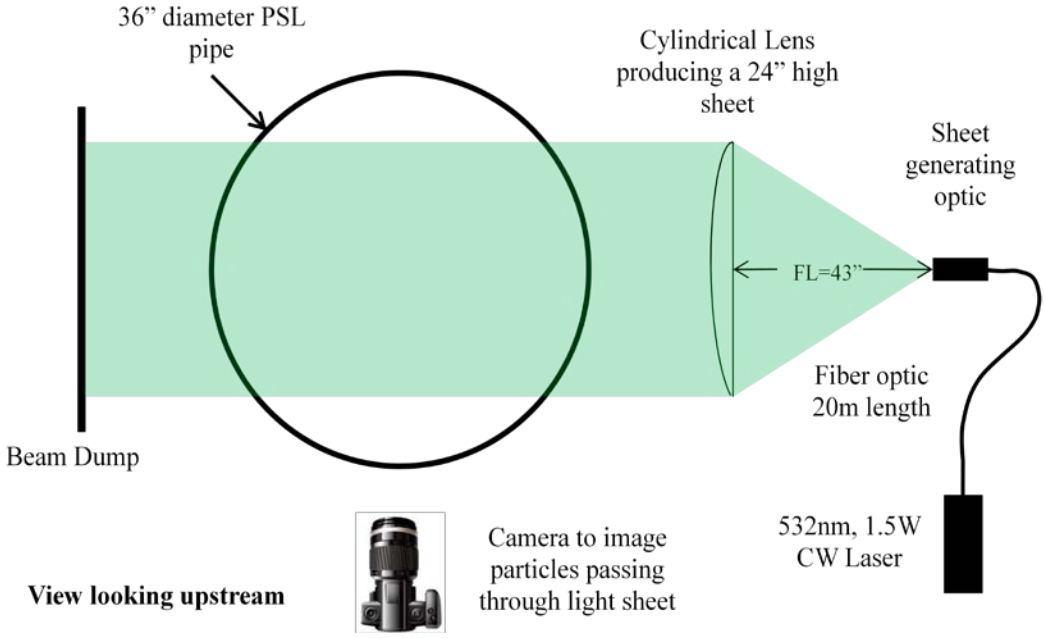

Figure 2. Schematic of the PSL laser sheet cloud imaging system.

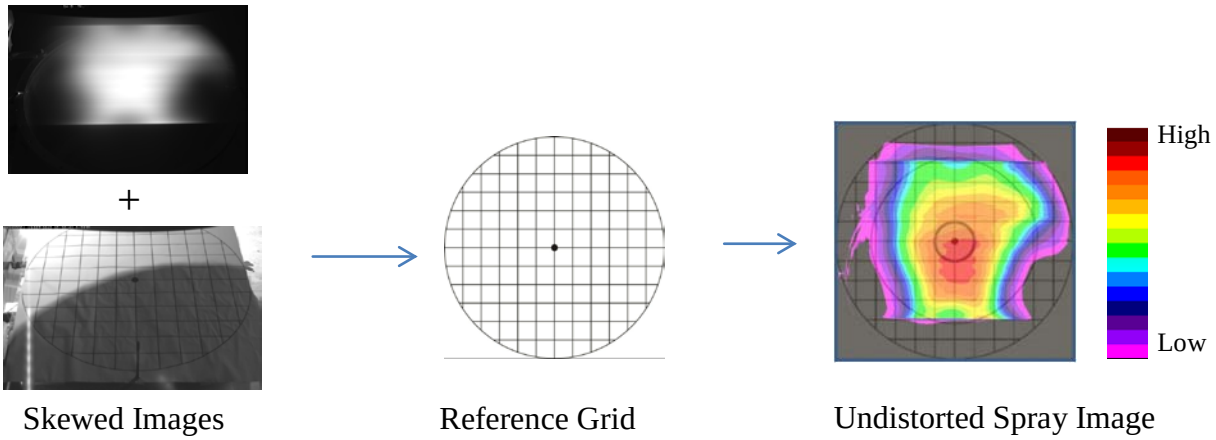

Figure 3. Image manipulation process for de-warping the laser sheet data images.

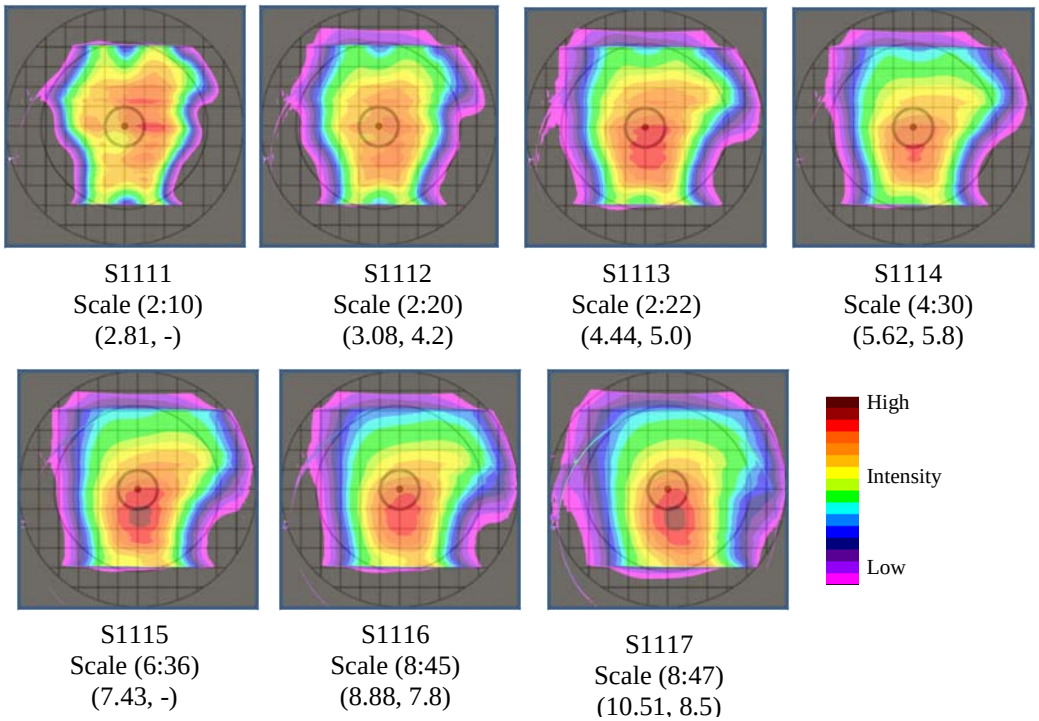

Figure 4. De-warped laser sheet image data from a series of seven sprays ranging from lightest (S1111) to heaviest (S1117). The scale (low:high) color intensity range varies from spray to spray and is noted below each image (units are counts/1000). The MVD ranged from 25 – 50 μm. Also noted are the preliminary cloud characteristics: (water injection in gpm, the measured center point TWC in g/m^3, if available). The outer circle of the overlaid grid indicates the 36" duct perimeter and the horizontal and vertical gridlines create 3" squares.

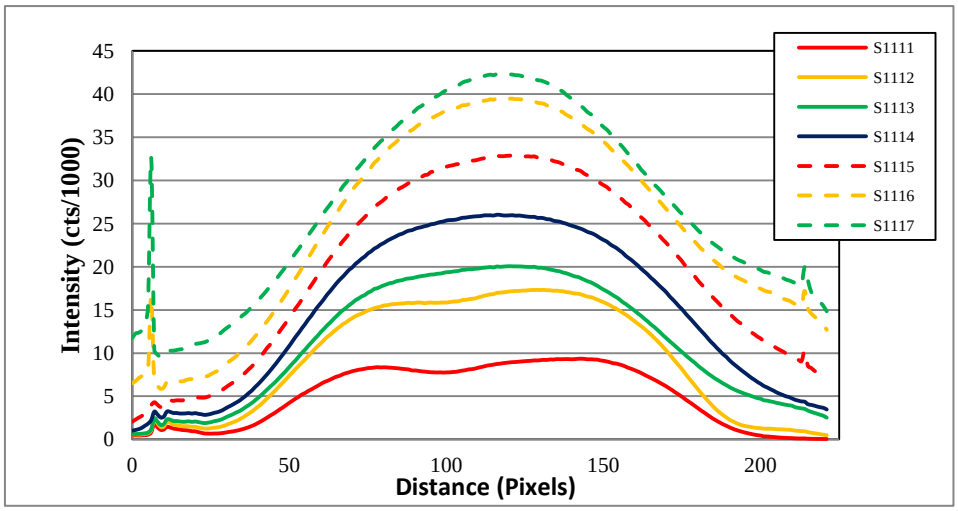

Figure 5. Horizontal profiles through the center of each spray in Figure 4 are shown in the line plot demonstrating the symmetry of the sprays and also the correlation between water content and image intensity.

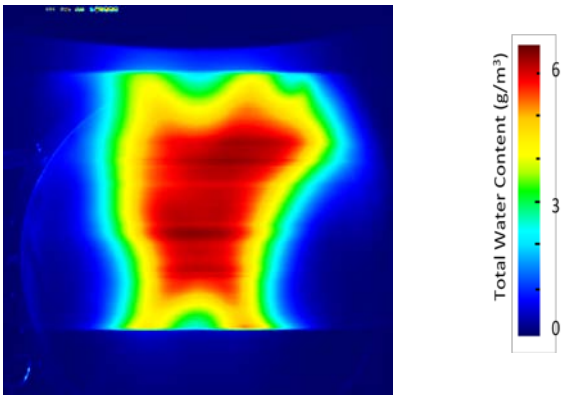

Figure 6. Laser sheet image data which has been calibrated against multi-wire or robust TWC probe measurements to provide quantitative TWC measurements.

III. Light Extinction Tomography

A light extinction tomography system was developed to provide an *in-situ* measurement system to monitor ice water clouds just upstream of a direct connected engine in the PSL facility. The tomography system provides qualitative and potentially quantitative full-field water content data in near real-time during engine testing in PSL with greater than a factor of three improvement in spatial resolution over existing (non-*in-situ*) instrumentation. To target the low-spatial-frequency nature of ice water clouds, unique computed tomography (CT) algorithms have been developed that use Gaussian basis functions rather than pixel basis functions typically used in medical and structural analysis applications. The attenuation model and reconstruction algorithms are detailed in the next section followed by a description of the instrument hardware and initial validation test results from a preliminary demonstration in the PSL facility.

A. Tomographic Algorithms

Tomographic reconstruction is the recovery of a quantity from a collection of line integrals of the quantity. The relevant quantity for this application is liquid water content. As discussed in Ref. 6, for the particle sizes expected in the PSL and the optical path lengths across the measurement section, the extinction of a beam of light passing through the spray will be proportional to the line integral of liquid water content along the optical path. In particular, the attenuation coefficient μ can be recovered from measurements of

$$-\ln\left(\frac{I}{I_0}\right) = \int_{l_i} \mu(x)ds \tag{1}$$

from a collection of lines l_i. Here, s denotes length along the line l_i from source to detector, I_0 is the source intensity, and I is the intensity measured on the detector. Measurements for I_0 are obtained for each source-detector pair by running the system without the spray being active.

The measurement model is essentially the same as that arising in medical CT. However, our application has several significant differences. To account for these differences, two different reconstruction algorithms were developed. In both medical applications and ours, the sources are in a ring outside the object and detectors are situated on a fan across from the source. However, in medical applications, the object of interest occupies a relatively small region about the center of the source ring. In the present application, the detectors are situated on the source ring, and the region of interest encompasses the entire interior of the PSL cross-section, (though the central region here is also of primary importance).

Because the reconstruction region extends to the source ring, the standard reconstruction algorithms used in a medical setting must be modified to avoid significant artifacts. Another difference is that our sample density is much lower, so the available resolution in the reconstruction of the spray will be relatively low. On the other hand,

since the spray itself is not expected to have sharp transitions, this is not expected to be a problem. Moreover, this *a priori* information can be exploited by modeling the spray as a superposition of Gaussian shaped blobs.

As an alternative to the traditional medical-type reconstruction, an algorithm has been developed which incorporates this *a priori* knowledge to reduce the computational complexity. It should be noted that the alternative algorithm does not scale well to the medical setting, but is well suited for use with the sampling densities available here. In this algorithm, the measurements are simulated for each possible Gaussian blob. The acquired spray measurement is fit to a linear combination of the simulated blob measurements. The corresponding linear combination of Gaussian blobs is taken as the reconstructed image. This method is easily adapted to handle minor malfunctions in the acquisition system such as a dark source, or a dead detector.

The other reconstruction algorithm which is used is a variant of the standard medical reconstruction algorithm known as filtered backprojection. The first step in our implementation is to reorganize the provided measurements to conform to those used in the medical setting. The sampling density determines the appropriate bandwidth to use as a parameter in the reconstruction computation. In order to reduce streaking artifacts, the sampled data are upsampled from 120×60 to 480×240. This upsampling preserves the original bandwidth of the data. The reconstruction is based on this original bandwidth and does not improve the resolution, even though the reconstruction is performed on a finer grid. Although this method does well in the central 2/3 of the field of view, it is not as robust in the outer ring due to the uneven coverage of source-detector paths through the outer ring, and also because the filtered backprojection algorithm relies on an approximation which is less valid at reconstruction points close to the source ring.

B. Prototype Tomography System Description

The light extinction tomography system consists of 60 equally spaced laser diodes with sheet generating optics and diffusing elements providing >300^{o} coverage around the ring and 120 fiber optically coupled detection elements mounted every 3^{o} around a 36” diameter ring. Photographs of the prototype system installed at the exit of the PSL piping are shown in Figure 7. Each detector utilizes a flashed opal input diffuser at the fiber entrance which is coupled to the CCD camera for simultaneous sampling of all 120 channels. The diffuser allows coupling of the laser light into the fibers at a very wide input angle of approximately +/- 85^{o} with respect to the fiber face. The diffusers greatly increase the acceptance angle of the fibers at the cost of allowing only a small amount of the incident light to be coupled into the fiber. The laser diode sources are pulsed sequentially while the detectors acquire line-of-sight extinction data for each laser pulse. A custom timing/triggering circuit was built in-house and used to control the data acquisition. The optical fibers are direct coupled to the CCD through a fiberoptic faceplate. The imaged fibers are read out as a 5×5 pixel binned region of interest in the center of the fiber which yields a pixel per fiber or a 120 pixel image per sequential laser scan. The optical fiber and detection system are shown in Figure 8.

Using the computed tomography algorithms discussed in the previous section the extinction data is used to produce a plot of the relative water content in the measurement plane with spatial resolution better than 1-inch over the central 75% of the measurement area. Figure 9 (left) illustrates the lines from several sources and the corresponding projections to the detectors. This gives some indication about the expected resolution as the area near the wall has a minimal amount of line crossing in multiple directions. A resolution study was performed to determine the expected resolution across the duct plane using simulated phantom data of 1 inch circles (center image) and performing the reconstruction of the simulated line projection information. The reconstruction of the 60 source, 120 detector configuration is shown in the right image illustrating the loss of resolution with increasing radial distance from the center of the duct. The 1 inch circles are clearly evident in the inner two rings which represent approximately a 12 inch diameter. The third ring of circles from the center are now turned into ovals which shows a loss of angular resolution but each dot can still be recognized, this corresponds to a diameter of approximately 20 inches. The outer most dots are completely blended together at approximately a 30 inch diameter. This study was performed using a high spatial frequency model because of the abrupt high contrast of the dots on the black background. This high spatial resolution leads to reconstruction artifacts which can be ignored since the intent of the study is to confirm the expected resolution and not to minimize the reconstruction noise.

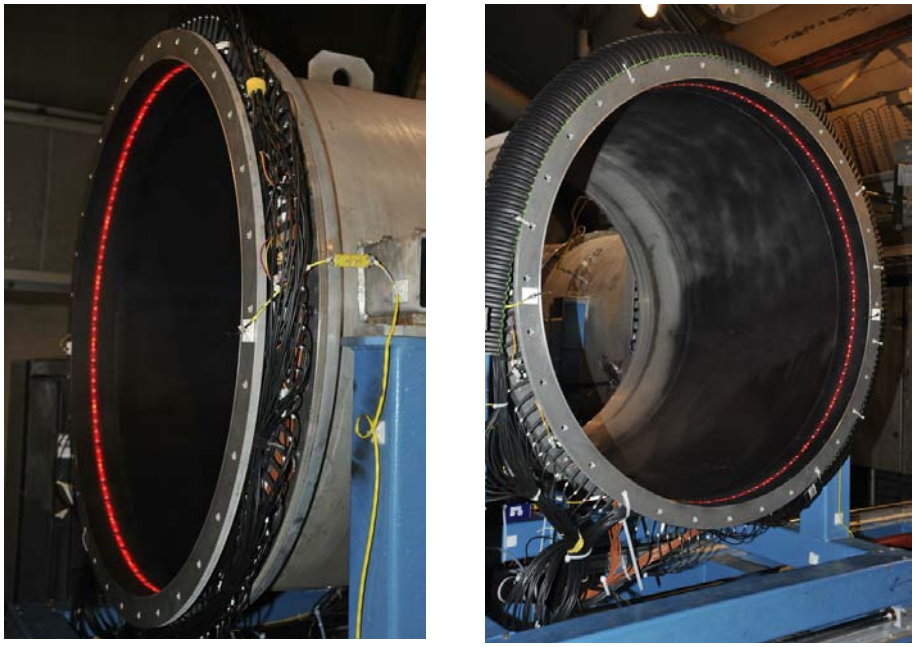

Figure 7. Photographs of the light extinction tomography prototype installed at the PSL pipe exit. The tomography spool section contains ports for 60 laser diode sources with sheet generating optics and diffusing elements that provide > 300^{o} coverage around the ring, and 120 optical fibers connections with high input angle optical elements. The optical fibers couple the transmitted light to a CCD detector (shown in Figure 8) enabling measurement of the light attenuation along the line of sight caused by the ice particles. Only 20 laser sources were used for the initial PSL demonstration due to limited laser availability at the time of the test.

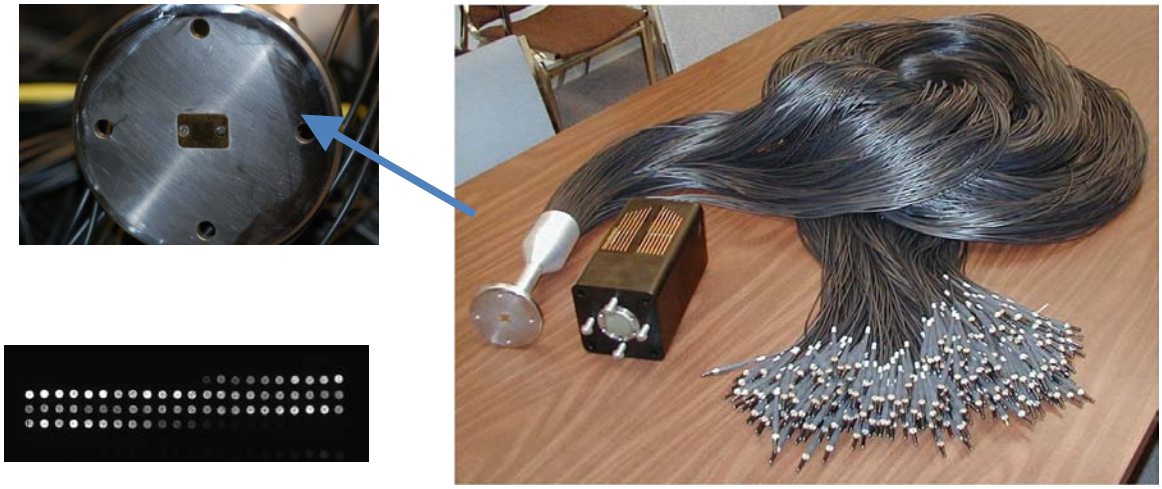

Figure 8. The detection system utilizes fiber coupling from the tomography spool to the camera to make the light intensity measurements. The fibers are "butted" directly to the CCD to give very high throughput and 16 bit sampling accuracy. The sample data image (lower left) shows the light collected by the 120 fibers from a single laser pulse of 1ms duration; not all fibers show signal since light is only coupled into the fibers within the ~300^{o} angular range of the light sheet from the specific light source that is active during the acquisition.

Figure 9. The projections for several sources to detectors coverage are demonstrated in the left image; a phantom image (center) used for a resolution study to demonstrate the resolution quality between the center of the ring and the outer regions near the wall of the ring; the reconstruction of the simulated data (right) assuming a 60 source, 120 detector configuration.

C. Tomography System Demonstration and Validation

Initial validation data were acquired during the PSL calibration test with the prototype tomography ring mounted to the exit of the PSL piping by mating flanges that were added to the unit as shown in Figure 7. The configuration tested had 120 equally spaced fiber optically coupled detectors around the entire circumference of the pipe. While the current system configuration has 60 laser fan sources, this validation test was performed with only 20 sources due to limited laser availability. The sources were mounted every 18^{o} and located between two detectors or shifted 1.5^{o} with respect to the detector pattern while remaining in the same axial plane. The laser pulse duration was controlled by camera exposure which was 1ms for all test points. A sequence was defined as the serial pulsing of all 20 lasers plus a dark reading for background subtraction while sampling all 120 detectors; this produced an image array that was 120×21 pixels. A sample raw image data array is shown in Figure 10. Thirty pre-spray reference sequences were acquired just prior to the ice cloud being turned on with the facility on condition for temperature and altitude. Once the ice cloud had been established, thirty spray sequences were acquired.

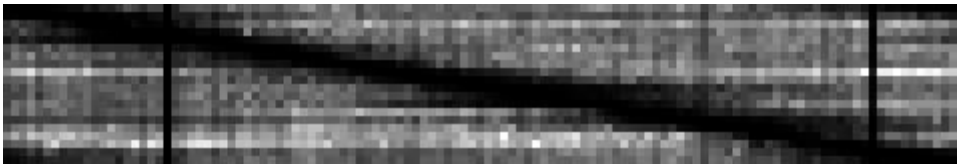

Figure 10. Sample raw data image where each row is a readout of all the detectors for a laser fan source turned on. The two dark columns have a much lower intensity but were still active for an extinction measurement.

Ten different spray conditions, shown in Table 1, were tested covering a minimal faulty nozzle condition to the maximum flow range in an attempt to verify the usefulness of the tomography system across the entire operating range of the PSL spray system. Figure 11 shows the horizontal centerline plots of the reconstruction images for all ten cases tested in the PSL. The sprays were characterized in three density categories as ‘light’ (S2960 series, dashed line), ‘medium’ (S2920 series, solid line) and ‘heavy’ (S2910 series, dotted line). The light sprays represent lower TWCs and the lowest number densities (# particles / cubic cm) of a typical spray condition. The MVD increased substantially in this series, going from approximately 34 µm in S2961 to over 300 µm in S2963. The minimal detectable sensitivity of the tomography system was evaluated by acquiring data from a spray that consisted of two “leaking” nozzles (S2929). The medium sprays had a constant particle size of 34µm and two different TWCs depending on the number of nozzles. For each set, two nozzles were turned off on one of the sprays of each set to observe the detection of a failed spray valve or plugged nozzle and the accompanying change in TWC amount and

distribution. The heavy sprays were to observe the effects of the maximum flow capability that the spraybars can produce and again the effects of failures of spray nozzles on the cloud just upstream of the location of an engine. The tomography system has sufficient sensitivity to easily detect the "leaking" nozzle condition as a minimal spray condition at 0.08 gpm as well as the maximum water supply condition at 8.2 gpm. The reconstructed image results of these extreme cases are shown in Figure 12 demonstrating that the tomography system has a very large TWC dynamic range capability.

Table 1. Spray conditions for tomography duct study. Estimates of MVD, ND and TWC provided if measured.

Test Point #	Pair (psid)	DeltaP (psid)	Nozzle #	Water Flow Rate (gpm)	MVD (est.) (um)	ND (est.) (#/cc)	TWC RP (est.) (g/m3)	Max Intensity (a.u.)	Comments
"Light Spray" 2960 series									
S2961	10	10	36	1.37	34	894	1.91	0.040	
S2963	10	25	36	2.16	200	692	3.69	0.039	
S2964	10	40	36	2.73	350	740	4.76	0.042	
"Medium Spray" 2920 series									
S2923	20	40	36	2.73	34	1923	3.36	0.089	
S2922	20	40	34	2.58	34	1923		0.085	Turn off 614 & 508
S2928	20	40	72	5.46	34		6.52	0.197	
S2927	20	40	70	5.31	34			0.193	Turn off 614 & 508
S2929	20	10	2	0.08				0.012	Leaky nozzle 818, 409
"Heavy Spray" 2910 series									
S2917	50	130	60	8.21	40	3500	8.00	0.356	
S2916	50	130	58	7.94	40	3500		0.348	Turn off 614 & 508

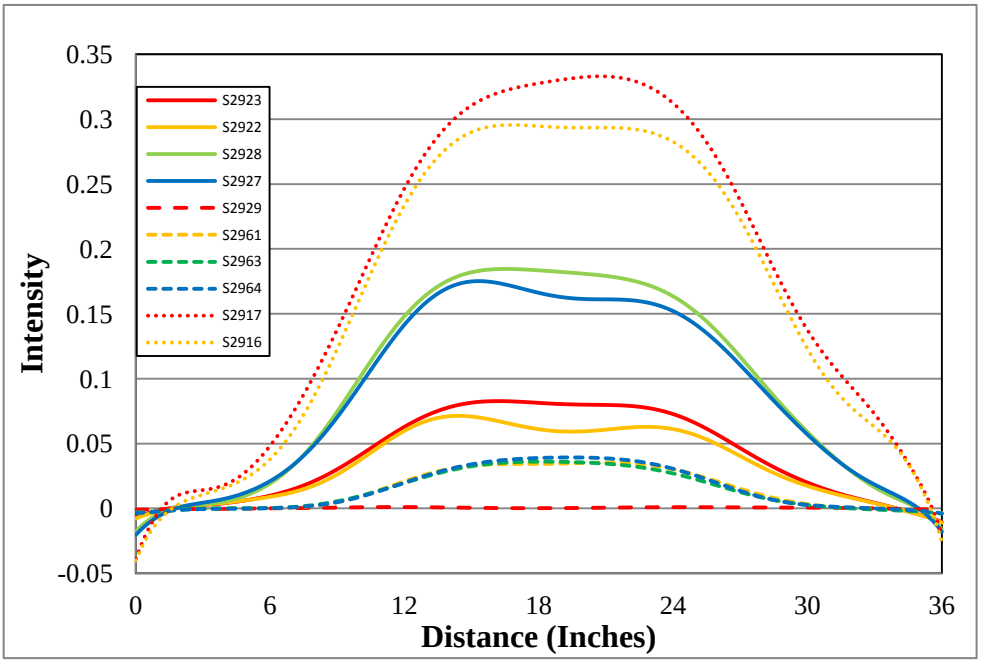

Figure 11. Horizontal centerline plots for the ten different spray conditions measured by the tomography system covering the minimum two "leaking" nozzles spray up to the maximum spray capability.

A potential cloud monitoring system capability that was tested was the ability to indicate changes in the flow from individual spray nozzles (e.g. the ability to monitor the loss of flow from a nozzle due to clogging or freezing up). Images from two distinct spray configurations were acquired; one with 30 nozzles active and one with only 28 of the 30 nozzles active as described above. As shown in Figure 13(a) and (b), the reconstructed images of the two spray configurations are very similar. However, a subtraction of the reconstructed images (Figure 13(c)) clearly shows the location of the two inactive nozzles, suggesting that the system has the capability to dynamically track the status of specific spray nozzles that may change during a spray.

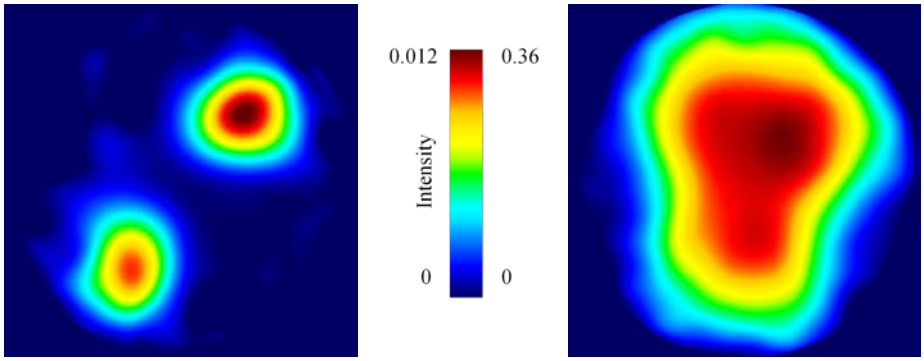

Figure 12. Examples of the extreme conditions from a minimal spray (S2929) with two nozzles on in a "leaking" condition at 0.08 gpm on the left and maximum spray (S2917) of the PSL spraybar system at 8.2 gpm on the right to evaluate the sensitivity of the tomography system as highlighted by the large difference in the maximum scale for the images.

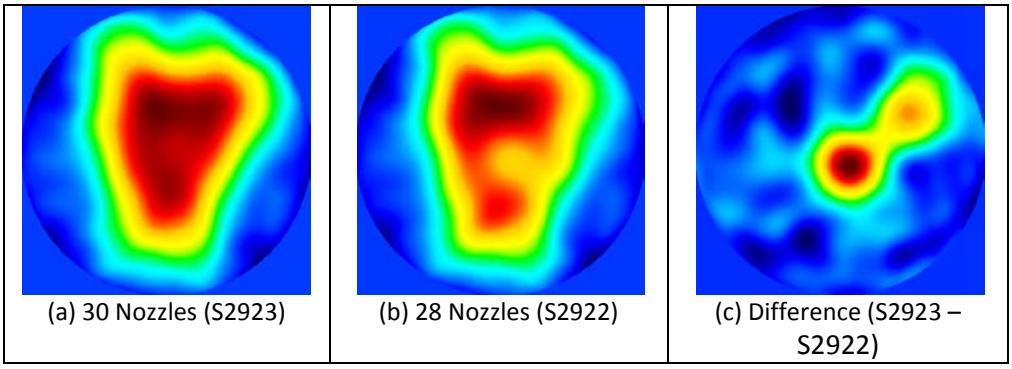

Figure 13. Reconstructed PSL images of a 30 nozzle ice cloud (a), a cloud with only 28 of the 30 nozzles active (b), and the difference between the two images (c) clearly showing the two inactive nozzle locations.

IV. Technique Comparison Study

A. Results

The tomography duct was installed and tested in PSL for only a very short duration at the end of the facility calibration at which time several calibration conditions from the laser sheet imaging data set were re-run to compare both optical detection systems. The comparison study used the corrected laser sheet images and the reconstructed tomography duct measurement intensity values. These measurements were scaled using the center-measured data obtained from the robust probe or multi-wire TWC probe measurement runs with the same facility and cloud conditions. The average value of the optical measurements over the center 1 inch area that corresponds to the robust

or multi-wire TWC measurement area was used to generate a linear relationship between optical intensity and the probe data. This created a ratio between a known TWC in the center duct as measured by the probes and laser or tomography reconstruction intensity that was then applied to the entirety of the measurement area to create the scaled planar TWC values. The bulk TWC value is an average of the center circular area of both the calibrated laser sheet and tomography TWC distributions. For the purposes of comparison, the diameter of the circle was the largest that the laser sheet will support, about 21.5 inches for spray S1865 and 23.5 inches for spray S2423. Figure 14 and Figure 15 show the TWC measured by the laser sheet and the tomography methods with the circle representing the area used to calculate the bulk TWC for each spray. The maximum TWC value in the table represents the greatest scaled value of sheet laser and tomography techniques which often does not occur in the center of the duct. The ratio of integrated bulk TWC from the planar optical techniques to the robust probe measurement is computed. This ratio indicates that the average TWC over the center approximately 22 inch diameter is about 70% of the value measured by the robust probe in the center one inch of the duct. The two techniques produce bulk TWC calculations that are in very good agreement for data acquired during different runs over several months. The bulk TWC to robust probe ratio gives an indication of the uniformity from the center point value.

The tomography data using the same calibration method described above was plotted for spray conditions having the same median particle size of 34μm. Figure 16 shows the linear relationship between the TWC measured by the probes and the reconstruction intensity for the 34μm particle size cases, as well as data for reconstructions of sprays with different particle median sizes. The drop size variation data shows a definite relationship of the tomography data with particle size as is assumed by the model which varies with number density and particle cross-sectional area. A complete calibration of the tomography system will be performed during the second facility calibration period prior to the next engine test currently scheduled for 2014.

B. Assessment

The laser sheet imaging technique is a very useful tool to qualitatively assess the liquid and ice sprays in the PSL facility. This non-intrusive technique is easy to install and setup, acquisition is fast and realistic assessment of spatial information is rapid. The cloud temporal response can be easily captured with the use of a video or high speed camera. The technique however is prone to reflections from surfaces near the laser light plane that can obscure the data especially at skewed imaging angles. The laser light sheet can be attenuated axially as it penetrates dense clouds and can suffer non-uniform light intensities from foreign objects on the optical surfaces along with optical fiber properties. Overall the laser sheet imaging is a very good tool to qualitatively and quantitatively assess ice crystal and liquid water clouds for uniformity and relative spatial densities. It should be noted that quantitative results from the laser sheet technique rely on having sufficient *a priori* knowledge of TWC and droplet size from a separate probe measurement at a point or region within the sheet laser measurement plane.

The light extinction tomography system has been demonstrated for limited cases but shows great potential to qualitatively asses the liquid and ice sprays in the PSL facility. This non-intrusive system is much more complicated in light source generation, light detection and data reduction but is much better at acquiring information in the closed duct area just upstream of an engine. The acquisition of reading out the fiber-coupled detectors for each pulsed laser source is significantly slower than the sheet laser method but limited temporal information may be possible using an interlaced method of detection. This system does not appear to suffer from scattering from surfaces or attenuation through the cloud as this is the light property of interest. The information in the center of the duct has higher spatial resolution than that at the wall but the center is of much higher interest; this could be minimized by increasing the number of laser fan sources around the circumference of the pipe. Overall, the tomography system with its limited actual testing appears to be the preferred method to quantitatively measure the amount and spatial distribution of the ice cloud without interfering with the flow upstream of a test engine in the PSL facility. As with the laser sheet technique, the tomography technique also relies on *a priori* knowledge of TWC and droplet size from a separate probe measurement at some point within the tomography measurement plane in order to provide quantitative results.

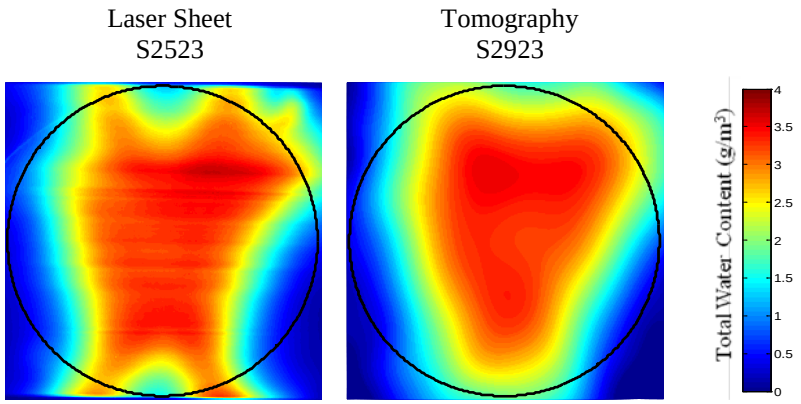

	TWC Circle Diameter	Robust Probe TWC	Bulk TWC	Max TWC	Bulk/Robust Ratio
Tomography	23.6"	3.295	2.439	3.587	74.0%
Laser Sheet	23.6"	3.295	2.440	3.743	74.1%

Figure 14. Comparison between the laser sheet and tomography methods for identical conditions, sampled on different dates. The center point robust probe measurement is S2423.

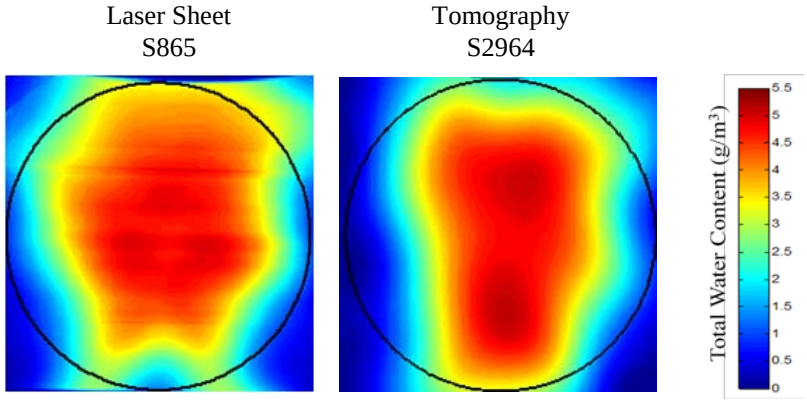

	TWC Circle Diameter	Robust Probe TWC	Bulk TWC	Max TWC	Bulk/Robust Ratio
Tomography	21.5"	4.787	3.255	5.152	68.0%
Laser Sheet	21.5"	4.787	3.454	5.023	72.1%

Figure 15. Comparison between the laser sheet and tomography methods for identical conditions, sampled on different dates. The center point robust probe measurement is S1865.

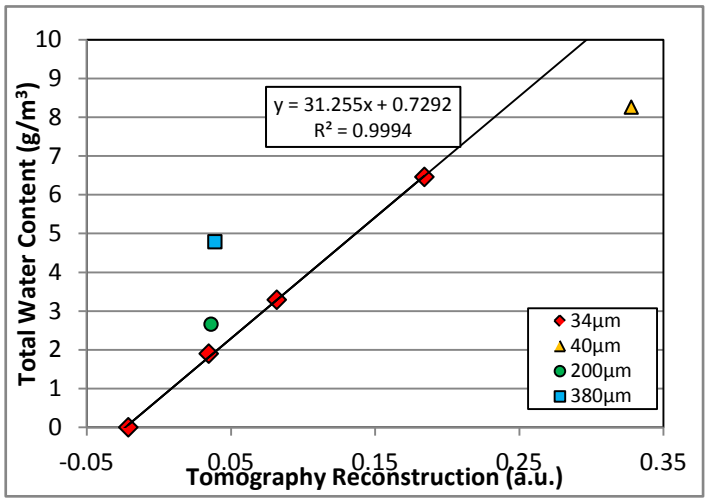

Figure 16. Tomography data which correlates the reconstruction center one inch region average with the multi-wire or robust TWC probe measurements. The three 34 micron sprays provide enough data for quantitative TWC measurements.

V. Conclusions and Future Work

The laser sheet imaging system has been successfully applied to provide cloud uniformity and water content measurements of the newly installed ice crystal cloud generation capability at the PSL facility. A series of increasing density sprays showed a very good correlation between imaged intensity and TWC. Single point multi-wire or robust TWC probe measurements were used to calibrate the image intensity to generate TWC maps. The laser sheet cloud calibration data was acquired prior to the installation of the light extinction tomography system and used as a means of providing validation information for comparison with the tomography results. A prototype light extinction tomography system has been tested in PSL using a wide range of sprays from a minimal spray system water flow rate of 0.08gpm to a maximum flow rate condition of 8.21gpm. This is the first ever application of light extinction tomography applied to ice crystal cloud measurement. Data obtained for several sprays having a MVD = 34µm show a linear relationship between reconstruction intensity and TWC as measured by the robust probe. Data analyzed for comparable sprays using the two optical techniques and the TWC probe measurements showed excellent agreement in calculating a bulk TWC averaged over a circular region in the center of the duct where both optical techniques data overlapped. A more complete calibration of the tomography system will be performed during the PSL facility calibration in the first quarter of 2014 where the online acquisition and reconstruction capabilities along with spray analysis tools will be demonstrated.

Acknowledgements

The authors would like to thank Trevor John for machining and building all of the tomography system hardware, Lawrence Greer for designing and building the laser timing/triggering circuit and Michelle Clem for supporting the laser sheet installation and test data acquisition. We would also like to thank the PSL facility technicians and engineers for their dedication and hard work in supporting this test. Finally, we would like to acknowledge NASA's Aviation Safety and Aeronautics Test Programs for supporting this work.

References

[1]Mason, J. G., Strapp, J. W., and Chow, P., "The Ice Particle Threat to Engines in Flight," AIAA-2006-206, 2006.

[2]Canacci, V. A., Bencic, T. J., Krupar, M. J., and Potapczuk, M. G., "A Sheet Laser Flow Visualization System in the NASA Lewis Icing Research Tunnel," AIAA-1998-0342, 1998.

[3]Bencic, T. J., "Development of Advanced Optical Instrumentation for Use in the NASA Glenn Icing Research Tunnel," AIAA-2001-0396, 2001.

[4]Halama, G. E., Ray, M. D., Anderson, K., Nesnidal, M. P., and Ide, R., “Optical Ice Detection: Test Results from the NASA Glenn Icing Research Tunnel,” AIAA-2010-7532, 2010.
[5]Papadakis, M., Hung, K. E., Vu, G. T., Bidwell, C. S., Breer, M. D., Bencic, T. J., “Experimental Investigation of Water Droplet Impingement on Airfoils, Finite Wings, and an S-Duct Engine Inlet,” NASA TM-2002-211700, 2002.
[6]Izen, S. H. and Bencic, T. J., “Application of the Radon Transform to Calibration of the NASA-Glenn Icing Research Wind Tunnel,” *Contemporary Mathematics*, Vol. 278, 2001, pp. 147-166.
[7]Van Zante, J. F., Ide, R. F., and Steen, L. E., “NASA Glenn Icing Research Tunnel: 2012 Cloud Calibration Procedure and Results," AIAA 2012-2933, 2012.